Numerical Modeling of Ultrasound Propagation in Weakly Heterogeneous Media Using a Mixed-Domain Method

Juanjuan Gu and Yun Jing, *Senior Member, IEEE*

***Abstract*— A mixed-domain method (MDM) is presented in this paper for modeling one-way linear/nonlinear wave propagation in biological tissue with arbitrary heterogeneities, in which sound speed, density, attenuation coefficients, and nonlinear coefficients are all spatial varying functions. The present method is based on solving an integral equation derived from a Westervelt-like equation. One-dimensional problems are first studied to verify the MDM and to reveal its limitations. It is shown that this method is accurate for cases with small variation of sound speed. A 2-D case is further studied with focused ultrasound beams to validate the application of the method in the medical field. Results from the MATLAB toolbox k-Wave are used as the benchmark. Normalized root-mean-square (rms) error estimated at the focus of the transducer is 0.0133 when the coarsest mesh (1/3 of the wavelength) is used in the MDM. Fundamental and second-harmonic fields throughout the considered computational domains are compared and good agreement is observed. Overall, this paper demonstrates that the MDM is a computationally efficient and accurate method when used to model wave propagation in biological tissue with relatively weak heterogeneities.**

***Index Terms*— Focused ultrasound, heterogeneous media, mixed-domain method (MDM), one-way propagation.**

I. Introduction

HIGH-INTENSITY focused ultrasound (HIFU) has received a great deal of attention in recent years due to its noninvasive characteristic. HIFU has been applied to treating a variety of diseases such as uterine fibroids [1], breast cancer [2], [3], brain tumor [4], stroke [5], and pancreatic cancer [6], [7]. One challenge to the expansion of HIFU technology is the need to fully understand and compensate for the potential of excessive heating and unwanted cavitation to damage healthy tissue. Fast, accurate characterization of the waveform and pressure distribution is crucial for both scientific investigation and clinical translation of HIFU techniques. Direct measurement of acoustic wave pressure and temperature fields inside tissue is extremely difficult and suffers from various types of hydrophone measurement errors and viscous heating artifacts when using thermocouples. Numerical acoustic wave propagation models can be utilized as an alternative or adjunctive approach to study the safety and effectiveness of HIFU devices under a broader range of conditions than can be investigated experimentally. Another advantage of numerical modeling is that it could facilitate treatment planning [8]–[10] and transducer design [11]–[13] with reduced cost when compared to experimental testing using real transducers.

During the last two decades, many studies have focused on numerical modeling of ultrasound propagation in tissue-like media. A time-domain numerical model is presented in [14] for studying HIFU in homogeneous media. Diffraction, nonlinearity, and absorption effects are treated independently using the method of fractional steps with a second-order operator-splitting algorithm. To investigate the pressure and temperature distribution from focused ultrasound, researchers have used a finite-difference time-domain (FDTD) method to model the propagation of a finite amplitude sound in homogeneous thermos-viscous fluids [15]. Though the finite-difference method is a powerful technique for modeling wave propagation, it can be time-consuming as very fine spatial and temporal resolutions may be required. Clement and Hynynen [16] investigated the forward and backward projection of linear acoustic fields in homogeneous media with the angular spectrum approach (ASA). A modified ASA was proposed and evaluated in [17] and [18] for homogeneous media with nonlinearity considered. However, these methods are not sufficient because they assume homogeneous media, but the biological tissue is heterogeneous and may have complicated geometries. This is confounded by the fact that the larger the transducer aperture (to achieve a sharper focusing), the stronger is the defocusing, since heterogeneities distort the wave front. The ability to capture the defocusing in a numerical model is critically important for HIFU safety evaluation.

A wide spectrum of wave solvers has been developed for modeling wave propagation in heterogeneous media. An iterative nonlinear contrast source method was developed [19] to model wave propagation in heterogeneous media. Liu [20] proposed a pseudospectral time-domain algorithm to solve large-scale problems for acoustic waves in multidimensional, heterogeneous, absorptive media. Varslot and Taraldsen [21] derived a one-way wave equation which permits smooth variation in all acoustically important variables. Both finite difference and angular spectrum methods are applied for numerical implementation. A second-order wave equation describing nonlinear wave propagation in

Manuscript received January 20, 2018; accepted April 16, 2018. Date of publication April 20, 2018; date of current version June 26, 2018. This work was supported in part by the U.S. National Institutes of Health under Grant R01EB025205. The work of J. Gu was supported by a fellowship from the China Scholarship Council. *(Corresponding author: Yun Jing.)*

The authors are with the Department of Mechanical and Aerospace Engineering, North Carolina State University, Raleigh, NC 27695 USA (e-mail: yjing2@ncsu.edu).

Digital Object Identifier 10.1109/TUFFC.2018.2828316

heterogeneous, attenuating media is solved numerically with the FDTD method by Pinton *et al.* [22]. An algorithm for modeling shock wave propagation in weakly heterogeneous and lossless media was proposed in [23]. A k-space time-domain method for modeling of wave propagation in heterogeneous media was investigated by Mast *et al.* [24] and was later extended to take nonlinear wave propagation into account [25], [26]. Clement and Hynynen [27] combined the ASA with ray theory to describe the propagation of ultrasound through randomly oriented, dissipative, layered media. Vyas and Christensen [28] modified the traditional ASA for simulating linear wave propagation in inhomogeneous media. For a more extensive literature review, the readers are referred to a recent reviewer paper [29].

This paper presents a mixed-domain method (MDM) for modeling linear/nonlinear wave propagation in dissipative, weakly heterogeneous media, which are considered good approximations for soft tissue. The methodology of MDM is presented in Section II. The method is based on solving a Westervelt-like equation, and it utilizes an implicit analytical solution derived by Jing *et al.* [17], [18]. The implicit analytical solution calculates results in the frequency domain and is able to model one-way wave propagation in soft tissue with variations in sound speed, density, attenuation coefficient, and nonlinearity coefficient. Two sets of problems are studied in this paper and are described in Section III. The first set of problems are 1-D problems. Four separate cases are studied: media with inhomogeneous speed of sound; media with inhomogeneous density; media with inhomogeneous attenuation; and media with inhomogeneous nonlinearity. Analytical solutions are used as benchmarks for the first two cases. Simulation results obtained from toolbox k-Wave [30] are used as the benchmark for the last two cases. The second set of problems are 2-D with focused ultrasound beams and involve a more realistic medium. The k-Wave results are used as the benchmark. To fully validate the accuracy of the MDM, we consider heterogeneities in the speed of sound, density, attenuation coefficient, and nonlinearity coefficient in a progressive manner. Results are compared in the time domain as well as in the frequency domain. Discussion and the conclusion can be found in Sections IV and V.

II. Governing Equation and Method

A Westervelt-like equation is first employed in this paper to describe the wave propagation in heterogeneous media [29]

$$\rho\nabla\cdot\left(\frac{1}{\rho}\nabla p\right)-\frac{1}{c^2}\frac{\partial^2 p}{\partial t^2}+\frac{\delta}{c^4}\frac{\partial^3 p}{\partial t^3}+\frac{\beta}{\rho c^4}\frac{\partial^2 p^2}{\partial t^2}=0 \quad (1)$$

where p is the acoustic pressure, ρ is the ambient density, c is the speed of sound, δ is the sound diffusivity, and $\delta = 2\alpha_{\mathrm{NP}}c^3/\omega^2$, where α_{NP} is the attenuation coefficient with unit Np/m, ω is the angular frequency; and β is the nonlinearity coefficient. All material parameters are spatially varying functions, providing great flexibility to the model. It was also demonstrated that the Westervelt equation is accurate for strongly focused transducers [31]. By applying the normalized wave field $= f\times\sqrt{\rho}$, (1) becomes

$$\nabla^2 f-\frac{1}{c^2}\frac{\partial^2 f}{\partial t^2}=f\sqrt{\rho}\nabla^2\frac{1}{\sqrt{\rho}}-\frac{\delta}{c^4}\frac{\partial^3 f}{\partial t^3}-\frac{\beta}{\sqrt{\rho}c^4}\frac{\partial^2 f^2}{\partial t^2}. \quad (2)$$

By performing the Fourier transform with respect to time t, (2) becomes

$$\nabla^2 F_t(f)+\tilde{k}^2F_t(f)=\sqrt{\rho}\nabla^2\frac{1}{\sqrt{\rho}}F_t(f)+\frac{i\delta\omega^3}{c^4}F_t(f)+\frac{\beta\omega^2}{\sqrt{\rho}c^4}F_t(f^2) \quad (3)$$

where F_t is the Fourier transform operator in the time domain and $\tilde{k}^2=\omega^2/c^2$. To satisfy both the power law attenuation and Kramers–Kronig dispersion relation [32]–[34], we have [35]

$$\tilde{k}=\frac{\omega}{c}-\frac{\alpha(-i)^{y+1}\omega^y}{\cos(\pi y/2)} \quad (4)$$

where y is the power law exponent. By neglecting the second-order attenuation terms and recognizing that $(-i)^y=\cos(\pi y/2)-i\sin(\pi y/2)$, the following equation can be obtained [36]:

$$\tilde{k}^2=\frac{\omega^2}{c^2}+\frac{2i\alpha\omega^{y+1}}{c}+\frac{2\alpha\tan(\pi y/2)\omega^{y+1}}{c}. \quad (5)$$

The imaginary part of (5) corresponds to the dispersion and the third term accounts for the attenuation. We drop the imaginary part in (5) as attenuation has already been considered in (1) or (2). Now (5) is simplified to

$$\tilde{k}^2=\frac{\omega^2}{c^2}+\frac{2\alpha\tan(\pi y/2)\omega^{y+1}}{c}. \quad (6)$$

Replacing $\tilde{k}^2$ in (3) with (6) yields

$$\nabla^2 F_t(f)+\left(\frac{\omega^2}{c^2}+\frac{2\alpha\tan(\pi y/2)\omega^{y+1}}{c}\right)F_t(f)=\sqrt{\rho}\nabla^2\frac{1}{\sqrt{\rho}}F_t(f)+\frac{i\delta\omega^3}{c^4}F_t(f)+\frac{\beta\omega^2}{\sqrt{\rho}c^4}F_t(f^2). \quad (7)$$

By performing an inverse temporal Fourier transform to (7), a wave equation satisfying Kramers–Kronig dispersion relation is given [35]

$$\nabla^2 f-\frac{1}{c^2}\frac{\partial^2 f}{\partial t^2}=f\sqrt{\rho}\nabla^2\frac{1}{\sqrt{\rho}}+\frac{2\alpha\tan(\pi y/2)}{c}\frac{\partial^{y+1}f}{\partial t^{y+1}}-\frac{\delta}{c^4}\frac{\partial^3 f}{\partial t^3}-\frac{\beta}{\sqrt{\rho}c^4}\frac{\partial^2 f^2}{\partial t^2}. \quad (8)$$

Alternatively, the Kramers–Kronig dispersion relation can be applied to (1) directly by replacing the speed of sound c with c_p and $c_p = (1/c+\alpha_0\tan(\pi y/2)(\omega^{y-1})^{-1}$, where $\alpha_0=\alpha_{\mathrm{NP}}\omega^{-y}$. Other models for dispersion and absorption are discussed in [35] and [37]–[41]. By performing Fourier

transform to (8) with respect to x, y, and t, we have

$$\frac{\partial^2}{\partial z^2}\tilde{F} + K^2\tilde{F} = F_{xy}\left\{\left[\sqrt{\rho}\nabla^2\frac{1}{\sqrt{\rho}} - \frac{\omega^2}{c_0^2}\left(\frac{c_0^2}{c^2} - 1\right) - \frac{2\alpha\tan(\pi y/2)\omega^{y+1}}{c} + \frac{i\delta\omega^3}{c^4}\right]F_t(f)\right\} + F_{xy}\left(\frac{\beta\omega^2}{\sqrt{\rho}c^4}F_t\left(f^2\right)\right) \quad (9)$$

where $\tilde{F}$ is the Fourier transform of f in x, y, and t, F_{xy} is the Fourier transform operator in x- and y-dimensions, c_0 is the background sound speed and

$$K^2 = \frac{\omega^2}{c_0^2} - k_x^2 - k_y^2 \quad (10)$$

where k_x and k_y are wavenumbers in x- and y-dimensions. For forward one-way propagation, the solution to (9) can be derived from the 1-D Green's function in an integral form [17], such that

$$\tilde{F}(z) = \tilde{F}(0)e^{iKz} + \frac{e^{iKz}}{2iK}\int_0^z e^{-iKz'}M(f(z'))dz' \quad (11)$$

where

$$M = F_{xy}\left\{\left[\sqrt{\rho}\nabla^2\frac{1}{\sqrt{\rho}} - \frac{\omega^2}{c_0^2}\left(\frac{c_0^2}{c^2} - 1\right) - \frac{2\alpha\tan(\pi y/2)\omega^{y+1}}{c} + \frac{i\delta\omega^3}{c^4}\right]F_t(f)\right\} + F_{xy}\left(\frac{\beta\omega^2}{\sqrt{\rho}c^4}F_t(f^2)\right). \quad (12)$$

By applying the inverse Fourier Transform to $\tilde{F}(z)$ in (11), the acoustic pressure p can be recovered by $f \times \sqrt{\rho}$. This method is an MDM because (11) indicates that operations are needed in both the real physical domain (x and y) and the wave-vector domain (k_x and k_y). Term $\sqrt{\rho}\nabla^2(1/\sqrt{\rho})$ in (12) accounts for the variation of density, followed by the terms that account for the variation of sound speed, attenuation, and dispersion. The last term in (12) outside the brace considers the variation of nonlinearity. Equation (11) can be solved with a Simpson-like integral [18], which is implemented in this paper. In this way, the acoustic fields on planes parallel to the xy plane can be extrapolated with a step size dz. One limitation of the proposed method is that when modeling media with inhomogeneous speed of sound, it is only accurate for weak heterogeneities (Appendix).

III. Simulation Results

A. 1-D Simulation Results

We first investigate a set of 1-D problems. Four separate cases are studied: media with inhomogeneous speed of sound; media with inhomogeneous density; media with inhomogeneous attenuation; and media with inhomogeneous nonlinearity. We use analytical solutions as benchmark solutions for the first two cases and k-Wave results as the benchmark for the last two cases. The k-Wave is a software package for simulating linear/nonlinear wave propagation using the k-space time-domain method [30]. A Gaussian modulated pulse is used and is expressed as

$$p_{\text{source}} = p_0\exp(-t^2 f_c^2/2)\sin(2\pi f_c t) \quad (13)$$

where $p_0 = 1$Pa is the magnitude of the pulse and the center frequency of the pulse f_c is 1 MHz. For a two-step stair-like medium with speed c_{m1} in the first half of the domain and c_{m2} in the second half and with a total propagation distance of z, the analytical solution is [42]

$$p_{\text{speed}} = T_c p_0\exp(-t_c^2 f_c^2/2)\sin(2\pi f_c t_c) \quad (14)$$

where $t_c = z/2c_{m1} + z/2c_{m2}$ and $T_c = 2c_{m2}/(c_{m1} + c_{m2})$. For a two-step stair-like medium with density ρ_{m1} in the first half of the domain and ρ_{m2} in the second half, sound speed of c, and a total propagation distance of z, the analytical solution is [42]

$$p_{\text{density}} = T_\rho p_0\exp(-t_\rho^2 f_c^2/2)\sin(2\pi f_c t_\rho) \quad (15)$$

where $t_\rho = z/c$ and $T_\rho = 2\rho_{m2}/(\rho_{m1} + \rho_{m2})$. The accuracy of the model is quantified by calculating the normalized root-mean-square (rms) error which is defined as [28]

$$\Delta_{\text{nrms}} = \sqrt{\frac{\sum_{i=1}^{N}|P_{\text{MDM}}(i) - P_{\text{benchmark}}(i)|^2}{N}} \quad (16)$$

where $p_{\text{MDM}}(i)$ and $p_{\text{benchmark}}(i)$ are normalized pressures calculated with the MDM and the benchmark method, respectively. N is the number of sampling points. In this 1-D case, results are obtained at a certain receiver location (21 mm away from the source) and the points are sampled in the time domain. Step size dz does not significantly affect the result for this special case with only one interface and it is chosen as $1/27\lambda$.

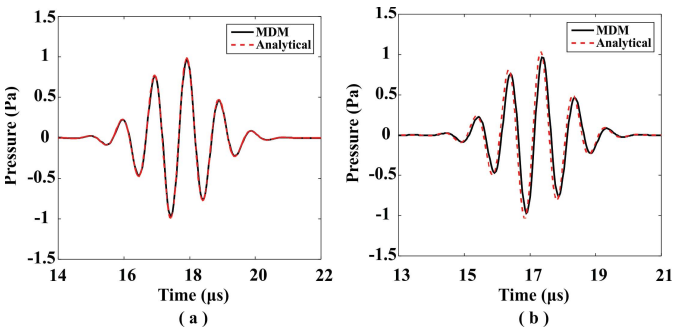

Fig. 1. Comparison between the MDM and analytical solution for the 1-D case with (a) weak sound speed contrast and (b) stronger sound speed contrast.

Fig. 1 illustrates the results for the wave propagation in a 1-D inhomogeneous medium with sound speed variation only. The total computational domain is 21 mm long. The received signal is recorded at the end of the computational domain. In Fig. 1(a), the sound speed for the first half of the computational domain is 1500 m/s, while it is 1575 m/s for the second half, indicating a relatively small contrast ratio of 1.05. In Fig. 1(b), the sound speed within the second

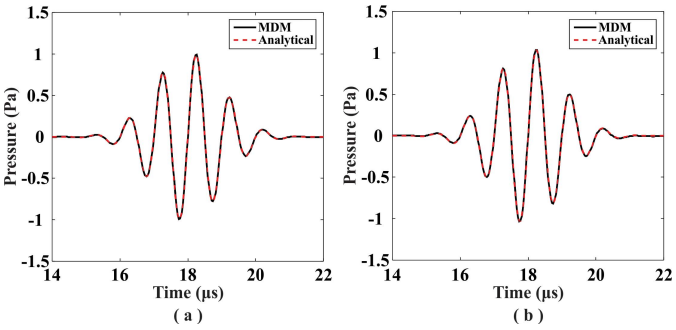

Fig. 2. Comparison between the MDM and analytical solution for the 1-D case with (a) weak density contrast and (b) stronger density contrast.

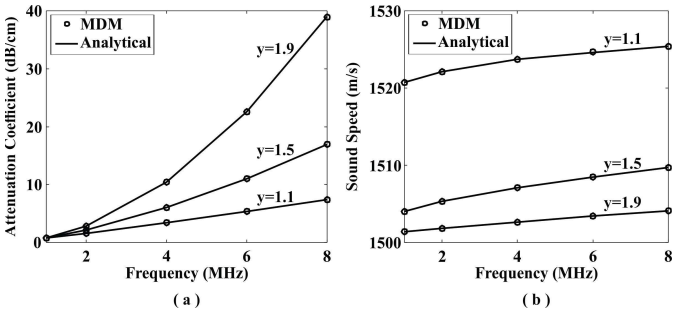

Fig. 3. (a) Attenuation coefficients and (b) frequency-dependent sound speed are obtained with the MDM at different frequencies for power law exponents of 1.1, 1.5, and 1.9. Analytical values are presented for comparisons.

half of the computational domain is increased to 1725 m/s, indicating a stronger contrast ratio of 1.15. Analytical solution for these two cases is (14). When wave propagates in the weakly heterogeneous medium, simulation results from the MDM are very close to the analytical results. More appreciable phase difference and amplitude difference can be observed in Fig. 1(b). In fact, the amplitude of the pulse remains almost unchanged for the MDM. These observations are consistent with the expectation that the MDM works better for weakly heterogeneous media and the transmission coefficient due to speed of sound variation is not considered (Appendix). On the other hand, the MDM does take the phase change into account, though the accuracy also depends on the contrast of the heterogeneity. The rms errors are 0.0135 and 0.1465 for the two cases, respectively. The proof that MDM currently works the best for weakly heterogeneous media (in speed of sound) is presented in the Appendix. It demonstrates that the MDM does not take the transmission coefficient due to sound speed variation into account, and the phase change is modeled most accurately when the sound speed contrast is low.

Fig. 2 records signals for the wave propagation in a 1-D inhomogeneous medium with density variation only. In Fig. 2(a), the density for the first half of the computational domain is 1000 kg/m^3, while at the second half is 1050 kg/m^3, indicating a relatively small contrast ratio of 1.05. In Fig. 2(b), the density within the second half of the computational domain is increased to 1150 kg/m^3, indicating a stronger contrast ratio of 1.15. Analytical solution for the two cases is (15). The rms errors for the cases with weak and stronger contrast are 0.0005 and 0.0052, respectively. Amplitudes of the main waveforms for the MDM and k-Wave results agree well for both weak and stronger contrast cases, indicating that the MDM does take the transmission coefficient into account in this case. The analytically predicted transmission coefficients for the two cases are 1.0243 and 1.0698, whereas the numerically estimated transmission coefficients are 1.0247 and 1.0636.

Attenuation and dispersion play very important roles in ultrasound propagation. While attenuation limits the depth that ultrasound can reach in tissues, dispersion can distort the waveform of ultrasound. The MDM considers both power law attenuation and Kramers–Kronig dispersion relation and can be readily used for modeling arbitrary dispersion and arbitrarily frequency-dependent attenuation as the algorithm operates in the frequency domain. To demonstrate the ability of the MDM to correctly model power law absorption and dispersion, the propagation of the Gaussian modulated wave through 1-D homogeneous absorbing media with different central frequencies ranging from 1 to 8 MHz is studied. In the simulation, the reference speed of sound is 1500 m/s and density is 1000 kg/m^3. The attenuation coefficient is chosen as 0.75 dB·MHz^{-y} · cm^{-1} for the whole domain. Attenuation coefficients and frequency-dependent sound speed are extracted from the time series recorded at two positions using the relations [36]

$$\alpha_{\mathrm{dB}} = -\frac{20\log_{10}(A_2/A_1)}{100d} \tag{17}$$

$$c_p = -\frac{\omega d}{\phi_2 - \phi_1} \tag{18}$$

where α_{dB} is the attenuation coefficient in unit of dB/cm, $A_{1,2}$ and $\phi_{1,2}$ are the single-sided amplitudes and phase spectra, d is the propagation distance in meters, and it is 0.005 m. Analytical values of the attenuation coefficient is calculated with $\alpha_{\mathrm{dB}} = \alpha f^y$, where α is in unit dB · MHz^{-y} · cm^{-1}; frequency-dependent sound speed is calculated with $1/c_p = 1/c_{\omega_0} + \alpha_0 \tan(\pi y/2)(\omega^{y-1} - \omega_0^{y-1})$, where ω_0 is chosen to be 1 MHz and the corresponding c_{ω_0} is extracted from the simulated data. Fig. 3(a) and (b) illustrates the attenuation coefficient and the sound speed as a function of frequency for power law exponents of 1.1, 1.5, and 1.9. Simulation and analytical results match very well. Results for the wave propagating in a 1-D medium with heterogeneity of attenuation coefficient are shown in Fig. 4. Attenuation coefficient at the first half domain is zero and is 1.5 dB · MHz^{-y} · cm^{-1} for the second half. The power law exponent y is 1.1. The normalized rms error is 0.0185, suggesting that both the loss and dispersion are accurately modeled.

The nonlinearity coefficient plays an important role in the distortion of waveform and the emergence of harmonics as the wave propagates. Media with nonlinearity parameter variation exhibit different nonlinear behaviors and it provides a potential route for ultrasound imaging [43]. Variation of nonlinearity coefficient has also been considered in our study and results are presented in Fig. 5. The pressure magnitude is increased to 4 MPa. The nonlinearity coefficient for the first half domain

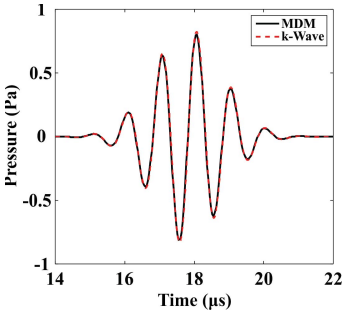

Fig. 4. Comparison between the MDM and k-Wave method for the 1-D case with attenuation coefficient variation.

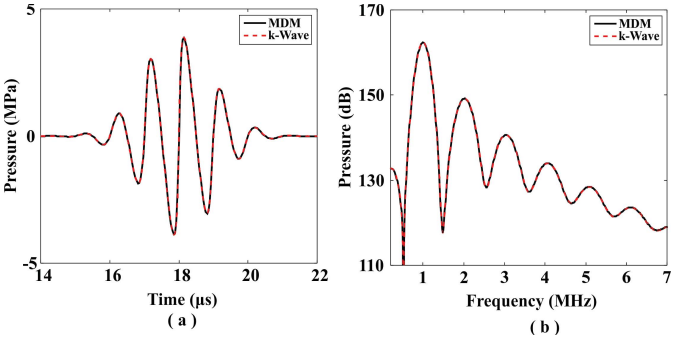

Fig. 5. Comparison between the MDM and k-Wave method for the 1-D case with nonlinearity coefficient variation. (a) Time-domain results. (b) Frequency-domain results.

TABLE I
TISSUE ACOUSTICAL PROPERTIES

	Speed of Sound m/s	Density kg/m^3	Attenuation coefficient $dB \cdot MHz^{-y} \cdot cm^{-1}$	Nonlinearity coefficient
Water	1500	1000	0.005	3.6
Fat	1480	937	0.40	5.8
Tumor	1563	1070	0.57	4.5

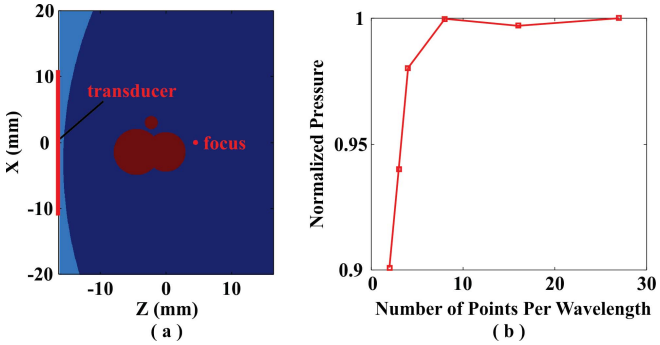

Fig. 6. (a) Geometry of the 2-D case. The computational domain shown here is cropped from the original domain for illustration purposes. The acoustical properties for different parts are listed in Table I. The light blue part is water; dark blue part represents the fat; three cylinders represent the tumors. The red line on the left indicates the array position. The red dot is the geometrical focus. (b) Convergence test for the MDM in the 2-D linear inhomogeneous medium with speed and density variations. The pressures at different spatial resolutions are recorded at the geometrical focus of the transducer and are normalized.

is 3.5, and is 5 for the second half. The normalized rms error is 0.0008. One additional simulation is carried out for MDM which considers a constant nonlinearity coefficient 3.5 for the whole domain. When compared with k-Wave with inhomogeneous nonlinearity coefficients, MDM with constant nonlinearity coefficient has larger normalized rms error and is 0.019. This suggests that the ability to model inhomogeneous nonlinearity coefficients does improve the accuracy of the simulation. Further details about nonlinear wave propagation are not discussed here since many studies on this topic have been carried out [44]–[48].

B. 2-D Simulation Results

A 2-D problem that is more realistic is further studied to verify the MDM. The same Gaussian modulated pulse is used. Pressure magnitude p_0 is 1 Pa when nonlinearity is not considered and is increased to 2 MPa when the nonlinear effect is investigated. The center frequency f_c is again 1 MHz. A planar phased array is used to model a focused beam. In both MDM and k-Wave, we define a phased array with phase delays in the source plane [17], [30], and we treat each cell in the source plane as a sound source with its individual phase delay. The geometrical focus is around 21 mm, and the aperture size is 22 mm. This configuration has variations in speed of sound, density, attenuation coefficient, and nonlinearity coefficient. It is used as a model to study the wave propagation from water to fat with tumors. Acoustic properties used in this model are listed in Table I. The power law exponent y is 1.1 throughout the computational domain. In theory, the power law exponent is two in water. However, k-Wave, which is used to generate benchmark solutions, cannot model problems that contain multiple values of power law exponent. Fig. 6(a) illustrates the geometry of the 2-D problem. The transverse dimension of the computational domain is 72.5 mm, and it is sufficiently large to reduce the wrap-around error [49]. It should be pointed out that absorption layers can be incorporated into the MDM to reduce the computational domain size [50]. Ultrasound wave propagates in the water (light blue) first and then penetrates the fat (dark blue). Tumors are represented with three cylinders, and their diameters are 3.5, 3.0, and 1.0 mm, respectively. Two of them have overlapped area. The reason why we choose simple geometries here is because later on we can easily vary the spatial resolution without changing the geometry of the problem. Both spatial step size and temporal step size used in the k-Wave are fine enough to obtain well-converged results. Spatial step sizes in the x- and y-directions are both $1/27\lambda$ (λ is the wavelength in fat and it is 1.48 mm at 1 MHz); the time step size is 4.6×10^{-4} μs. The corresponding Courant–Friedrichs–Lewy (CFL) number is 0.0123. The reason we choose such a small CFL number here is because a solution that is as accurate as possible is desired for benchmark. In addition, a convergence study is carried out on k-Wave and some slight phase errors at larger CFL numbers are observed and we want to minimize these errors. We investigate the accuracy of the MDM by varying the spatial step size dz. In addition, for simplicity, it is assumed that $dx = dz$, though in theory they could be different.

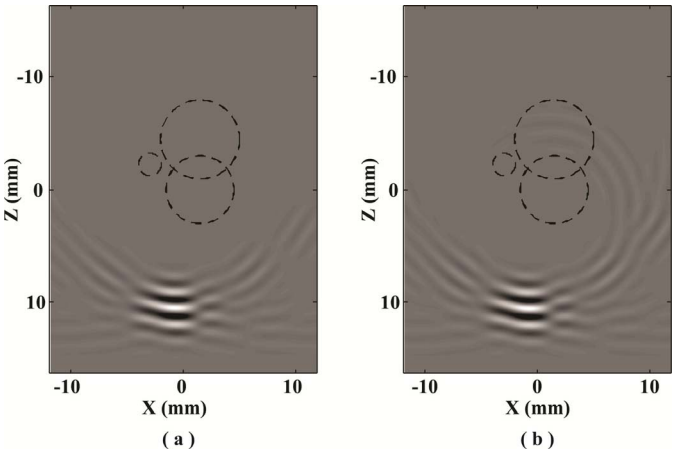

Fig. 7. Snapshots of the acoustic fields for the case with speed and density variations at $t = 22$ μs. The focused beam is simulated with the (a) MDM and (b) k-Wave. Dashed lines show the positions of the tumors.

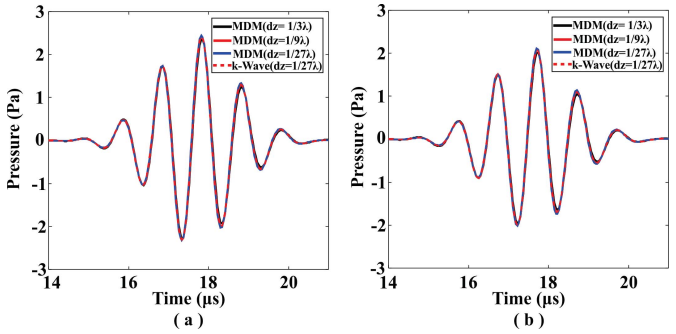

Fig. 8. Comparison between the MDM and k-Wave simulation results in the 2-D linear inhomogeneous medium with speed and density variations and (a) without attenuation and dispersion and (b) with attenuation and dispersion. Receiver location is at the geometrical focus of the transducer.

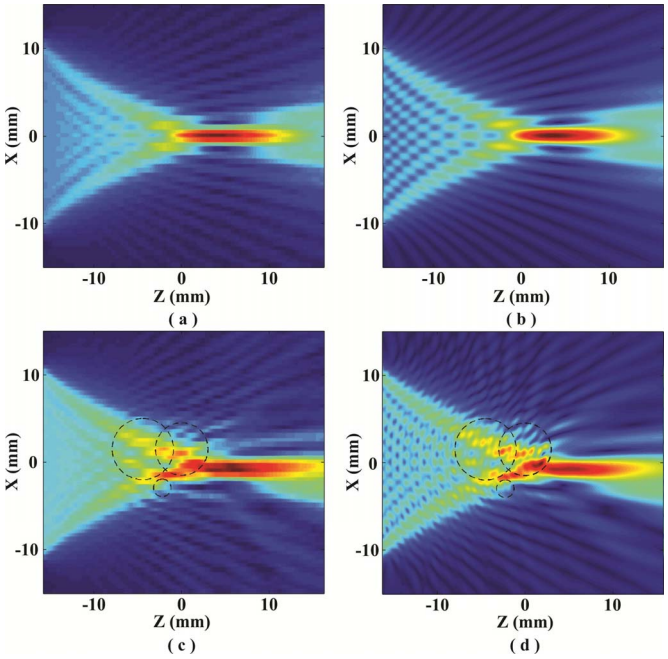

Fig. 9. Frequency-domain results for the fundamental frequency (1 MHz) in the homogeneous medium with (a) MDM and (b) k-Wave. Frequency-domain results for the fundamental frequency in the heterogeneous medium with (c) MDM and (d) k-Wave with speed of sound, density, and attenuation.

For the MDM, three spatial step sizes are selected and they are $1/3\lambda$, $1/9\lambda$, and $1/27\lambda$. The temporal resolution dt is fixed at 0.037 μs and additional simulations show that different dt does not significantly affect the result once the Nyquist sampling rate is well satisfied. The temporal domain size (end time) is 44 μs for all cases.

We first compare the results with speed and density variations only. A convergence test is conducted for this 2-D case at the geometrical focus of the transducer, and the result is shown in Fig. 6(b). The normalized pressure $P_{\text{normalized}}$ [51] is calculated with the formula $P_{\text{normalized}} = P_f/P_{27}$, where P_f is the pressure at the focus of the transducer with different numbers of points per wavelength, and P_{27} is the pressure at the same point when $dx = dz = 1/27\lambda$. Reasonably accurate results can be found starting at $1/4\lambda$. Acoustic fields for this case at $t = 22\mu$s are shown in Fig. 7. It is noted that the MDM result does not contain reflections due to the one-way approximation. However, the amplitude of the reflection is relatively small compared to transmission in soft biological tissue [21]. The waveforms at the focus are plotted in Fig. 8(a) for further comparison. From the comparison for the 1-D case [shown in Fig. 2(b)], we know that the MDM can predict accurate results even with relatively strong density variation. Thus, the amplitude and phase differences in Fig. 8(a) are mainly from the variation of speed of sound.

Next, attenuation and dispersion effects are added to the medium. The results are displayed in Fig. 8(b) and the phase and amplitude of the received signal are changed compared to the lossless case. The amplitude is evidently smaller due to the attenuation. Fig. 9 exhibits the frequency-domain results at 1 MHz. Spatial step size for MDM in Fig. 9 is $1/3\lambda$. For comparison, the results for the homogeneous case (water only) are also included. Even for the homogeneous case, some near-field discrepancy between the MDM and k-Wave can be observed, which is possibly due to different boundary conditions used in these two methods: the MDM uses the pressure release surface, whereas the k-Wave uses the Kirchhoff (or free field) boundary condition. However, differences from the boundary conditions in the far-field are negligible. For the heterogeneous case, some "ripples" are visible in the tumors in Fig. 9(d), which are not observed in Fig. 9(c). These features are due to the multiple scattering/reflection which is not considered in the present MDM. Nevertheless, the beam distortion looks very similar between the MDM and k-Wave results.

Afterwards, nonlinearity is considered. The nonlinearity coefficient is directly responsible for the increase of the harmonics in wave propagation. Results are compared in the time domain [Fig. 10(a)] and frequency domain [Fig. 10(b)]. Normalized rms errors evaluated at the geometrical focus are listed in Table II for all spatial resolutions trialed and the errors in general reduce (though not significantly) as the spatial resolution becomes finer. Note that the entire time-domain signal is used for computing the error although Figs. 8 and 10(a) only

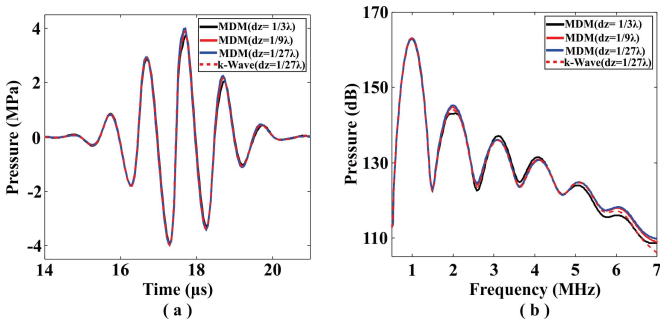

Fig. 10. Comparison between the MDM and k-Wave in a 2-D nonlinear lossy medium with speed and density variations in the (a) time domain and (b) frequency domain. Receiver location is at the geometrical focus of the transducer.

TABLE II
NORMALIZED RMS ERRORS

Spatial step size	$1/3\lambda$	$1/9\lambda$	$1/27\lambda$
Lossless medium	0.0109	0.0041	0.0040
Lossy medium	0.0111	0.0052	0.0036
Lossy medium with nonlinearity	0.0133	0.0073	0.0062

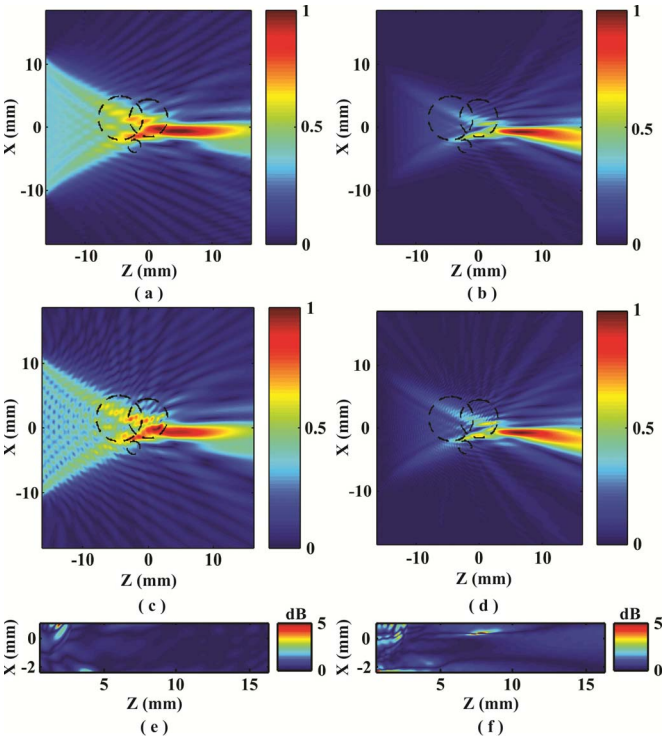

Fig. 11. Pressure for the (a) fundamental and (b) second-harmonic field simulated by the MDM. Pressure for the (c) fundamental and (d) second-harmonic field simulated by k-Wave. (e) and (f) Difference from the fundamental and second-harmonic components between the two methods around the transducer focal region. The MDM results shown here are with a spatial step size of $1/27\lambda$.

show the primary waveform (i.e., first-order transmission). Comparisons for the fundamental and second-harmonic frequency fields are shown in Fig. 11. The acoustic pressure fields in Fig. 11 are normalized. Fig. 11(e) and (f) shows the differences for the fundamental and second-harmonic components between the MDM and k-Wave in the focal region in unit dB. Normalized rms errors in the focal region are 0.0280 for the fundamental frequency field and 0.0149 for the second-harmonic field at the spatial resolution of $1/27\lambda$.

IV. DISCUSSION

Results from k-Wave are used as the benchmark solution in this paper, and the accuracy of k-Wave has been well documented in many papers [26], [36], [51]. The difference between MDM and k-Wave is expected to be due to a combination of different factors, including: 1) numerical errors of each method; 2) different model equations; and 3) different boundary conditions. Since very fine spatial and temporal resolutions are used, numerical errors from k-Wave should be minimized. While the MDM solves a second-order partial differential equation (PDE), the k-Wave solves a set of coupled first-order PDEs. For lossless cases though, it was shown that the second-order PDE can be derived from the coupled PDEs [26]. When considering loss, there is a slight difference in our method and k-Wave for the attenuation part. This error should be relatively small as evidenced by Fig. 4. There is also a difference in terms of setting up the boundary condition in k-Wave and our model, which has been briefly discussed. This difference mainly exists in the near field. The MDM has an intrinsic error of not including the reflection (due to one-way propagation), which should be the main contribution to the difference between the two methods. Reflections can be added to the MDM to improve the accuracy. One possible approach is to use the method proposed in [28]. Although the method in [28] only applies to linear waves, it should be sufficient since reflection in soft tissue has relatively low amplitude and therefore the nonlinear effect is weak.

To fully validate the MDM, two cases are studied. In the 1-D case, we investigate the accuracy of the MDM by considering the variations of sound speed, density, and attenuation separately. Results from the 1-D case show that this algorithm can predict accurate results in weakly heterogeneous medium. Afterwards, a set of 2-D problems are further studied. Variations of sound speed, density, attenuation, and nonlinearity are added step by step. Density variation and sound speed variation are first considered together. It is found that more accurate results can be obtained when the spatial resolution is finer. This is because a smaller step size (dx and dz) will reduce the error from stair-stepped surfaces [52] caused by discrete meshes. Stair-casing errors occur when representing complex geometries (like circular/spherical) with rectilinear grids. Reference [51] specifically studied this error for k-Wave and it is shown to be the most serious error when modeling transcranial ultrasound. The truncation error introduced by the numerical integration [53] will also be reduced if a smaller step size (dz) is used. However, even with a very coarse spatial resolution (i.e., $1/3\lambda$), the error of the MDM can still be kept small (on the order of 0.01). This is a great advantage when compared with the most commonly used FDTD scheme which requires 8–10 grid points per wavelength to achieve reasonably

accurate results. Besides, spatial aliasing error due to finite-domain size is also a possible source of error in the MDM. We have used sufficiently large x-axis range to minimize the spatial aliasing error.

The numerical implementation throughout this paper is based on MATLAB 2015b (The MathWorks Inc., Natick, MA, USA) on a 64-bit operating system with a quad-core 3.60-GHz Intel Xeon 5687 CPU (Intel Corp., Santa Clara, CA, USA) processors and 192 GB of RAM. For the linear 2-D case, the MDM with spatial step size $1/3\lambda$ takes 0.013 s to obtain the frequency-domain result shown in Fig. 9(c). With the same spatial step size and computational domain and a CFL number of 0.11, the k-Wave simulation needs 8.81 s, indicating a 677–fold computation speed difference. This computational difference is expected to be highly problem-dependent though and should not be generalized. The drastically different computation times are due to the fact that for k-Wave simulations, the time-domain simulation needs to be carried out first and the Fourier transform is performed to obtain the results at the frequency of interest. On the other hand, the MDM directly operates in the frequency domain and therefore can be considerably more efficient in producing frequency-domain results. This is particularly useful for modeling thermal-based HIFU problems since in many cases the frequency-domain results are of utmost importance.

V. Conclusion

An MDM is presented in this paper. The MDM solves the Westervelt-like equation with appropriate assumptions, and it is accurate for weakly heterogeneous media. Since the theory is presented for the general 3-D case, the algorithm, though only demonstrated in 1-D and 2-D, can be readily extended to modeling 3-D problems. In this paper, we have shown that the MDM is an efficient and accurate algorithm for modeling medical ultrasound propagating in soft tissue. There are many foreseeable applications for numerical modeling of ultrasound using the MDM. For example, it can assist HIFU device sponsors in preparing reliable preclinical testing data generated from computational modeling or facilitate HIFU treatment planning. Furthermore, ultrasound computed tomography (USCT) is an emerging imaging modality to reconstruct the sound speed, density, and attenuation of soft tissue for diagnosis through transmission signals [54]–[56]. However, computation time is one of the most critical issues for USCT. The computationally efficient MDM, therefore, can be proven to be a promising approach for frequency-domain USCT. In the future, we aim to modify the MDM so that it can be applied to strongly heterogeneous media, e.g., skull. Reflection will also be included to improve the accuracy.

Appendix

In this appendix, we will show that the MDM is valid for inhomogeneous media with weak sound speed contrast. To simplify the problem, we choose a scenario with a 1-D inhomogeneous medium with speed of sound variation only and the change occurs at the boundary where $z = z_0$. The medium is defined as

$$c = \begin{cases} c_0, & z \le z_0 \\ c_1, & z > z_0. \end{cases} \tag{A1}$$

For 1-D wave propagation, the solution for a point in the $z > z_0$ domain obtained from (11) is

$$P(z) = P_0 e^{ikz} + \frac{e^{ikz}}{2ik}\int_0^{z_0} e^{-ikz'}\left(-\frac{\omega^2}{c_0^2}\left(\frac{c_0^2}{c^2}-1\right)P(z')\right)dz' + \frac{e^{ikz}}{2ik}\int_{z_0}^{z} e^{-ikz'}\left(-\frac{\omega^2}{c_0^2}\left(\frac{c_0^2}{c^2}-1\right)P(z')\right)dz' \tag{A2}$$

where $k = \omega/c_0$. The second term in (A2) is zero with the speed distribution described in (A1). Thus, (A2) can be simplified to

$$P(z) = P_0 e^{ikz} + \frac{e^{ikz}}{2ik}\int_{z_0}^{z} e^{-ikz'}\left(-\frac{\omega^2}{c_0^2}\left(\frac{c_0^2}{c_1^2}-1\right)P(z')\right)dz'. \tag{A3}$$

On the other hand, the analytical solution for wave propagating in 1-D cases with sound speed shown in (A1) reads

$$P(z) = \begin{cases} P_0 e^{ikz}, & z \le z_0 \\ T P_0 e^{ikz_0 + ik'(z-z_0)}, & z > z_0 \end{cases} \tag{A4}$$

where $k' = \omega/c_1$ and T is the transmission coefficient and $T = 2c_1/(c_0 + c_1)$. Now we look at the wave field when $z > z_0$. If (A3) was valid, substituting (A4) into the right-hand side of (A3) will precisely lead to $P(z)$, i.e., $T P_0 e^{ikz_0 + ik'(z-z_0)}$. Therefore, we substitute (A4) into the right-hand side of (A3), which leads to

$$\begin{aligned} &P_0 e^{ikz} + \frac{e^{ikz}}{2ik}\int_{z_0}^{z} e^{-ikz'}\left(-\frac{\omega^2}{c_0^2}\left(\frac{c_0^2}{c_1^2}-1\right)T P_0 e^{ikz_0 + ik'(z-z_0)}\right)dz' \\ &= P_0 e^{ikz}\left(1 + T\frac{e^{i(k-k')z_0}}{2ik}\left(\frac{\omega^2}{c_0^2}-\frac{\omega^2}{c_1^2}\right)\int_{z_0}^{z} e^{i(k'-k)z'}dz'\right) \\ &= P_0 e^{ikz}\left(1 + T\frac{e^{i(k-k')z_0}}{2ik}\left(k^2 - k'^2\right)\int_{z_0}^{z} e^{i(k'-k)z'}dz'\right) \\ &= P_0 e^{ikz}\left(1 + e^{i(k-k')z_0}(e^{i(k'-k)z} - e^{i(k'-k)z_0})\right) \\ &= P_0 e^{ikz}\left(1 + e^{i(k-k')(z_0-z)} - 1\right) \\ &= P_0 e^{ikz_0 + ik'(z-z_0)}. \end{aligned} \tag{A5}$$

From (A5), we can conclude that the transmission coefficient T caused by the sound speed variation is not included in the MDM. In fact, if we multiplied (A3) with T, substituting (A4) into (A3) would precisely lead to $P(z) = T P_0 e^{ikz_0 + ik'(z-z_0)}$. This is not a major issue if the contrast in the medium is weak, since phase distortion will likely dominate over amplitude change.

Next, we focus on the accuracy of the phase when modeling wave propagation using the MDM. For convenience, we use the Riemann sum as the stepping algorithm [17]. With the left-hand Riemann sum, the MDM method for the 1-D case

with variation of speed of sound (the same case as above) can be written as

$$P(z+\Delta z)_{\mathrm{MDM}} = P(z)e^{ik\Delta z} + \frac{e^{ik\Delta z}}{2ik}\left(-\frac{\omega^2}{c_0^2}\left(\frac{c_0^2}{c_1^2}-1\right)\right)P(z)\Delta z. \quad \text{(A6)}$$

When wave propagates a distance of $z_0+\Delta z$, the pressure field becomes

$$P(z_0+\Delta z)_{\mathrm{MDM}} = P_0 e^{ik(z_0+\Delta z)}\left(1+\frac{k^2-k'^2}{2ik}\Delta z\right). \quad \text{(A7)}$$

When assuming weakly inhomogeneous medium, we have $k \approx k'$. Equation (A7) can be further simplified as

$$P(z_0+\Delta z)_{\mathrm{MDM}} \cong P_0 e^{ik(z_0+\Delta z)}[1+i(k'-k)\Delta z]. \quad \text{(A8)}$$

When the wave travels a distance of $z_0+\Delta z$, the analytical solution is

$$P(z_0+\Delta z)_{\mathrm{Analytical}} = T P_0 e^{ikz_0+ik'\Delta z}. \quad \text{(A9)}$$

By using the Euler's formula, (A9) becomes

$$P(z_0+\Delta z)_{\mathrm{Analytical}} = T P_0 e^{ik(z_0+\Delta z)}[\cos(k'\Delta z - k\Delta z) + i\sin(k'\Delta z - k\Delta z)]. \quad \text{(A10)}$$

When taking a rather small spatial step size Δz and considering that $k \approx k'$, we have $(k'-k)\Delta z \approx 0$. Equation (A10) becomes

$$P(z_0+\Delta z)_{\mathrm{Analytical}} = T P_0 e^{ik(z_0+\Delta z)}[1+i(k'-k)\Delta z]. \quad \text{(A11)}$$

Comparing (A11) and (A8), it is seen that the phase difference between MDM and the analytical solution is 0 when certain assumptions are made. Thus, the MDM is accurate in weekly heterogeneous media.

REFERENCES

[1] A. H. Chan, V. Y. Fujimoto, D. E. Moore, R. W. Martin, and S. Vaezy, "An image-guided high intensity focused ultrasound device for uterine fibroids treatment," *Med. Phys.*, vol. 29, no. 11, pp. 2611–2620, 2002.

[2] F. Wu *et al.*, "A randomised clinical trial of high-intensity focused ultrasound ablation for the treatment of patients with localised breast cancer," *Brit. J. Cancer*, vol. 89, no. 12, pp. 2227–2233, 2003.

[3] F. Wu *et al.*, "Extracorporeal high intensity focused ultrasound treatment for patients with breast cancer," *Breast Cancer Res. Treat.*, vol. 92, no. 1, pp. 51–60, Jul. 2005.

[4] J. Jagannathan *et al.*, "High-intensity focused ultrasound surgery of the brain: Part 1—A historical perspective with modern applications," *Neurosurgery*, vol. 64, no. 2, pp. 201–211, 2009.

[5] A. Burgess, Y. Huang, A. C. Waspe, M. Ganguly, D. E. Goertz, and K. Hynynen, "High-intensity focused ultrasound (HIFU) for dissolution of clots in a rabbit model of embolic stroke," *PLoS ONE*, vol. 7, no. 8, p. e42311, 2012.

[6] T. D. Khokhlova and J. H. Hwang, "HIFU for palliative treatment of pancreatic cancer," *J. Gastrointestinal Oncol.*, vol. 2, no. 3, pp. 175–184, 2011.

[7] H. J. Jang, J.-Y. Lee, D.-H. Lee, W.-H. Kim, and J. H. Hwang, "Current and future clinical applications of high-intensity focused ultrasound (HIFU) for pancreatic cancer," *Gut Liver*, vol. 4, pp. S57–S61, Sep. 2010.

[8] R. J. McGough, M. L. Kessler, E. S. Ebbini, and C. A. Cain, "Treatment planning for hyperthermia with ultrasound phased arrays," *IEEE Trans. Ultrason., Ferroelect., Freq. Control*, vol. 43, no. 6, pp. 1074–1084, Nov. 1996.

[9] L. Wu, V. Amin, R. Roberts, and T. Ryken, "An interactive HIFU therapy planning using simulation & visualization," in *Proc. AIP Conf.*, 2007, pp. 150–156.

[10] Y. Jing, F. C. Meral, and G. T. Clement, "Time-reversal transcranial ultrasound beam focusing using a k-space method," *Phys. Med. Biol.*, vol. 57, no. 4, p. 901, 2012.

[11] D. Pajek and K. Hynynen, "The design of a focused ultrasound transducer array for the treatment of stroke: A simulation study," *Phys. Med. Biol.*, vol. 57, no. 15, p. 4951, 2012.

[12] O. M. Al-Bataineh, C. M. Collins, E.-J. Park, H. Lee, and N. B. Smith, "MR thermometry characterization of a hyperthermia ultrasound array designed using the k-space computational method," *Biomed. Eng. Online*, vol. 5, no. 1, p. 56, 2006.

[13] X. Zeng, J. Li, and R. J. McGough, "A waveform diversity method for optimizing 3-D power depositions generated by ultrasound phased arrays," *IEEE Trans. Biomed. Eng.*, vol. 57, no. 1, pp. 41–47, Jan. 2010.

[14] J. Tavakkoli, D. Cathignol, R. Souchon, and O. A. Sapozhnikov, "Modeling of pulsed finite-amplitude focused sound beams in time domain," *J. Acoust. Soc. Amer.*, vol. 104, no. 4, pp. 2061–2072, 1998.

[15] I. M. Hallaj and R. O. Cleveland, "FDTD simulation of finite-amplitude pressure and temperature fields for biomedical ultrasound," *J. Acoust. Soc. Amer.*, vol. 105, no. 5, pp. L7–L12, 1999.

[16] G. Clement and K. Hynynen, "Field characterization of therapeutic ultrasound phased arrays through forward and backward planar projection," *J. Acoust. Soc. Amer.*, vol. 108, no. 1, pp. 441–446, 2000.

[17] Y. Jing, M. Tao, and G. T. Clement, "Evaluation of a wave-vector-frequency-domain method for nonlinear wave propagation," *J. Acoust. Soc. Amer.*, vol. 129, no. 1, pp. 32–46, 2011.

[18] Y. Jing, M. Tao, and J. Cannata, "An improved wave-vector frequency-domain method for nonlinear wave modeling," *IEEE Trans. Ultrason., Ferroelect., Freq. Control*, vol. 61, no. 3, pp. 515–524, Mar. 2014.

[19] L. Demi, K. van Dongen, and M. Verweij, "A contrast source method for nonlinear acoustic wave fields in media with spatially inhomogeneous attenuation," *J. Acoust. Soc. Amer.*, vol. 129, no. 3, pp. 1221–1230, 2011.

[20] Q. H. Liu, "The pseudospectral time-domain (PSTD) algorithm for acoustic waves in absorptive media," *IEEE Trans. Ultrason., Ferroelect., Freq. Control*, vol. 45, no. 4, pp. 1044–1055, Jul. 1998.

[21] T. Varslot and G. Taraldsen, "Computer simulation of forward wave propagation in soft tissue," *IEEE Trans. Ultrason., Ferroelect., Freq. Control*, vol. 52, no. 9, pp. 1473–1482, Sep. 2005.

[22] G. F. Pinton, J. Dahl, S. Rosenzweig, and G. E. Trahey, "A heterogeneous nonlinear attenuating full-wave model of ultrasound," *IEEE Trans. Ultrason. Ferroelect., Freq. Control*, vol. 56, no. 3, pp. 474–488, Mar. 2009.

[23] F. Dagrau, M. Rénier, R. Marchiano, and F. Coulouvrat, "Acoustic shock wave propagation in a heterogeneous medium: A numerical simulation beyond the parabolic approximation," *J. Acoust. Soc. Amer.*, vol. 130, no. 1, pp. 20–32, 2011.

[24] T. D. Mast, L. P. Souriau, D.-L. Liu, M. Tabei, A. I. Nachman, and R. C. Waag, "A k-space method for large-scale models of wave propagation in tissue," *IEEE Trans. Ultrason., Ferroelect., Freq. Control*, vol. 48, no. 2, pp. 341–354, Mar. 2001.

[25] Y. Jing, T. Wang, and G. T. Clement, "A k-space method for moderately nonlinear wave propagation," *IEEE Trans. Ultrason., Ferroelect., Freq. Control*, vol. 59, no. 8, pp. 1664–1673, Aug. 2012.

[26] B. E. Treeby, J. Jaros, A. P. Rendell, and B. Cox, "Modeling nonlinear ultrasound propagation in heterogeneous media with power law absorption using a k-space pseudospectral method," *J. Acoust. Soc. Amer.*, vol. 131, no. 6, pp. 4324–4336, 2012.

[27] G. T. Clement and K. Hynynen, "Forward planar projection through layered media," *IEEE Trans. Ultrason., Ferroelect., Freq. Control*, vol. 50, no. 12, pp. 1689–1698, Dec. 2003.

[28] U. Vyas and D. Christensen, "Ultrasound beam simulations in inhomogeneous tissue geometries using the hybrid angular spectrum method," *IEEE Trans. Ultrason., Ferroelect., Freq. Control*, vol. 59, no. 6, pp. 1093–1100, Jun. 2012.

[29] J. Gu and Y. Jing, "Modeling of wave propagation for medical ultrasound: A review," *IEEE Trans. Ultrason., Ferroelect., Freq. Control*, vol. 62, no. 11, pp. 1979–1992, Nov. 2015.

[30] B. E. Treeby and B. T. Cox, "k-Wave: MATLAB toolbox for the simulation and reconstruction of photoacoustic wave fields," *J. Biomed. Opt.*, vol. 15, no. 2, p. 021314, 2010.

[31] Y. Jing, D. Shen, and G. T. Clement, "Verification of the Westervelt equation for focused transducers," *IEEE Trans. Ultrason., Ferroelect., Freq. Control*, vol. 58, no. 5, pp. 1097–1101, May 2011.

[32] K. R. Waters, M. S. Hughes, J. Mobley, and J. G. Miller, "Differential forms of the Kramers-Kronig dispersion relations," *IEEE Trans. Ultrason., Ferroelect., Freq. Control*, vol. 50, no. 1, pp. 68–76, Jan. 2003.
[33] K. R. Waters, J. Mobley, and J. G. Miller, "Causality-imposed (Kramers-Kronig) relationships between attenuation and dispersion," *IEEE Trans. Ultrason., Ferroelect., Freq. Control*, vol. 52, no. 5, pp. 822–823, May 2005.
[34] J. Mobley, K. R. Waters, and J. G. Miller, "Causal determination of acoustic group velocity and frequency derivative of attenuation with finite-bandwidth Kramers-Kronig relations," *Phys. Rev. E, Stat. Phys. Plasmas Fluids Relat. Interdiscip. Top.*, vol. 72, no. 1, p. 016604, 2005.
[35] J. F. Kelly, R. J. McGough, and M. M. Meerschaert, "Analytical time-domain Green's functions for power-law media," *J. Acoust. Soc. Amer.*, vol. 124, no. 5, pp. 2861–2872, 2008.
[36] B. E. Treeby and B. Cox, "Modeling power law absorption and dispersion for acoustic propagation using the fractional Laplacian," *J. Acoust. Soc. Amer.*, vol. 127, no. 5, pp. 2741–2748, 2010.
[37] T. L. Szabo, "Time domain wave equations for lossy media obeying a frequency power law," *J. Acoust. Soc. Amer.*, vol. 96, no. 1, pp. 491–500, 1994.
[38] T. L. Szabo, "Causal theories and data for acoustic attenuation obeying a frequency power law," *J. Acoust. Soc. Amer.*, vol. 97, no. 1, pp. 14–24, 1995.
[39] W. Chen and S. Holm, "Modified Szabo's wave equation models for lossy media obeying frequency power law," *J. Acoust. Soc. Amer.*, vol. 114, no. 5, pp. 2570–2574, 2003.
[40] M. G. Wismer, "Finite element analysis of broadband acoustic pulses through inhomogenous media with power law attenuation," *J. Acoust. Soc. Amer.*, vol. 120, no. 6, pp. 3493–3502, 2006.
[41] S. P. Näsholm and S. Holm, "Linking multiple relaxation, power-law attenuation, and fractional wave equations," *J. Acoust. Soc. Amer.*, vol. 130, no. 5, pp. 3038–3045, 2011.
[42] L. E. Kinsler, A. R. Frey, A. B. Coppens, and J. V. Sanders, *Fundamentals of Acoustics*, 4th ed. Hoboken, NJ, USA: Wiley, Dec. 1999, ch. 6, sec. 2, pp. 150–152.
[43] F. Varray, O. Basset, P. Tortoli, and C. Cachard, "CREANUIS: A nonlinear radiofrequency ultrasound image simulator," *Ultrasound Med. Biol.*, vol. 39, no. 10, pp. 1915–1924, 2013.
[44] R. J. Zemp, J. Tavakkoli, and R. S. C. Cobbold, "Modeling of nonlinear ultrasound propagation in tissue from array transducers," *J. Acoust. Soc. Amer.*, vol. 113, no. 1, pp. 139–152, 2003.
[45] F. Varray, A. Ramalli, C. Cachard, P. Tortoli, and O. Basset, "Fundamental and second-harmonic ultrasound field computation of inhomogeneous nonlinear medium with a generalized angular spectrum method," *IEEE Trans. Ultrason., Ferroelect., Freq. Control*, vol. 58, no. 7, pp. 1366–1376, Jul. 2011.
[46] P. V. Yuldashev and V. A. Khokhlova, "Simulation of three-dimensional nonlinear fields of ultrasound therapeutic arrays," *Acoust. Phys.*, vol. 57, no. 3, pp. 334–343, May 2011.
[47] W. Kreider *et al.*, "Characterization of a multi-element clinical HIFU system using acoustic holography and nonlinear modeling," *IEEE Trans. Ultrason., Ferroelect., Freq. Control*, vol. 60, no. 8, pp. 1683–1698, Aug. 2013.
[48] V. A. Khokhlova *et al.*, "Design of HIFU transducers to generate specific nonlinear ultrasound fields," *Phys. Procedia*, vol. 87, pp. 132–138, Dec. 2016.
[49] X. Zeng and R. McGough, "Evaluation of the angular spectrum approach for simulations of near-field pressures," *J. Acoust. Soc. Amer.*, vol. 123, no. 1, pp. 68–76, Jan. 2008.
[50] Y. Jing, "On the use of an absorption layer for the angular spectrum approach (L)," *J. Acoust. Soc. Amer.*, vol. 131, no. 2, pp. 999–1002, 2012.
[51] J. L. Robertson, B. T. Cox, J. Jaros, and B. E. Treeby, "Accurate simulation of transcranial ultrasound propagation for ultrasonic neuromodulation and stimulation," *J. Acoust. Soc. Amer.*, vol. 141, no. 3, pp. 1726–1738, 2017.
[52] A. C. Cangellaris and D. B. Wright, "Analysis of the numerical error caused by the stair-stepped approximation of a conducting boundary in FDTD simulations of electromagnetic phenomena," *IEEE Trans. Antennas Propag.*, vol. 39, no. 10, pp. 1518–1525, Oct. 1991.
[53] D. L. Phillips, "A technique for the numerical solution of certain integral equations of the first kind," *J. ACM*, vol. 9, no. 1, pp. 84–97, 1962.
[54] G. Y. Sandhu, C. Li, O. Roy, S. Schmidt, and N. Duric, "Frequency domain ultrasound waveform tomography: Breast imaging using a ring transducer," *Phys. Med. Biol.*, vol. 60, no. 14, p. 5381, 2015.
[55] M. Pérez-Liva, J. Herraiz, J. Udías, E. Miller, B. T. Cox, and B. E. Treeby, "Time domain reconstruction of sound speed and attenuation in ultrasound computed tomography using full wave inversion," *J. Acoust. Soc. Amer.*, vol. 141, no. 3, pp. 1595–1604, 2017.
[56] K. Wang, T. Matthews, F. Anis, C. Li, N. Duric, and M. A. Anastasio, "Waveform inversion with source encoding for breast sound speed reconstruction in ultrasound computed tomography," *IEEE Trans. Ultrason., Ferroelect., Freq. Control*, vol. 62, no. 3, pp. 475–493, Mar. 2015.

Juanjuan Gu received the B.S. degree in energy and power engineering from Jiangsu University, Zhenjiang, China, in 2014. She is currently pursuing the Ph.D. degree with the Department of Mechanical and Aerospace Engineering, North Carolina State University, Raleigh, NC, USA.

Her research focuses on numerical modeling of ultrasound wave propagation.

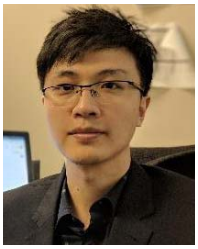

Yun Jing (S'08–M'10–SM'17) received the B.S. degree in electronic science and engineering from Nanjing University, Nanjing, China, in 2006, and the M.S. degree and the Ph.D. degree in architectural acoustics from Rensselaer Polytechnic Institute, Troy, NY, USA, in 2007 and 2009, respectively.

He was a Research Fellow with Brigham and Womens Hospital, Harvard Medical School, Boston, MA, USA. He is currently with the Faculty of North Carolina State University, Raleigh, NC, USA, where he was promoted to an Associate Professor in 2017. He specializes in the development of analytic and numerical methods for linear and nonlinear wave propagation in fluids. He has published over 50 peer-reviewed scientific manuscripts. He is interested in biomedical ultrasound, acoustic metamaterials, architectural acoustics, nonlinear acoustics, and noise control.

Dr. Jing is an Elected Member of the Technical Committee of the IEEE Ultrasonics (TPC 3). He was a recipient of the 2018 R. Bruce Lindsay Award from the Acoustical Society of America.